Prediction of Sound Propagation in Long Enclosures with Different Impedance Boundaries Using Coherent Model

Jacob Chia-chun Liu[1]，Po-Chien Lu，Luke Chen

Abstract

A theoretical model has been developed for the prediction of sound propagation in a rectangular long enclosure. The model is based on the image-source method, and the effect of interference among the infinite number of image sources generated by multiple reflections is incorporated by coherently summing the contributions from the image sources. The various impedances of the boundaries are added in the model. Experiments are carried out to validate the proposed theoretical model, where the enclosure walls are lined with different kinds of sound absorption material to simulate different impedance boundaries. It is shown in the paper that the developed model agrees reasonably better with the experimental data than that of the ODEON software.

Keywords: Sound propagation; long enclosures with different impedance boundaries using coherent model

[1] *Department of Water Resources and Environmental Engineering*
Tamkang University Taiwan

1. Introduction

All acoustic features of the long enclosure need to be considered for noise control in highway or railway tunnels, sound interference control in corridors of public buildings, and increase of speech intelligibility of the broadcasting systems in the subway station. In the field of acoustics, a long enclosure is defined as a three-dimensional enclosure where the length of one dimension is over three times longer than that of the other two dimensions. The sound field has been assumed to be diffuse in traditional theories of room acoustics. Under this assumption, the original distribution regularity and reverberation regularity of the sound field are not perfectly applicable to the long enclosure [1]. Therefore, the acoustic phenomena and regularities in the long enclosure need more specific researches. There have been researches on the sound field in long enclosures since the 1960s [2]. Since the 1970s, many scholars have continually conducted researches on various acoustic properties in the long enclosure with the image source method [3-5]. All the image source methods used in these researches have been based on geometric acoustics. In the 1990s, Lemire et al. used the complex wave theory-based image source model to solve the problem of sound propagation among finite boundaries in a long enclosure [6]. In 2004, Li et al. used the complex image source model in research of the sound propagation in long enclosures and indicated that the fact that the early stage theoretic model tend to neglect the effects of interference due to multiple reflections of sound rays from boundary walls in the long enclosure, hence the previous simulative predictions were not very accurate because of the interferences [7]. Li et al. proposed to sum up the effect of interference and the effect of the image source to obtain a coherent model which predict sound field in the long enclosure. The experimentally measured attenuation levels of the sound pressure at different frequencies at a fixed location in the long enclosure are different, which is in line with the theories. On the basis of Li's research, this paper has actualized a coherent model of a long enclosure and studied the sound attenuation along the long axis direction of a long enclosure with different impedance boundaries with the model.

2.Theory

As shown in Fig. 1, the width of the long enclosure is *W* and the height is *H*, with the ground situated at a plane of $z = 0$. The two vertical walls that are perpendicular to the ground are situated at $x = 0$ and $x = W$ respectively. The locations of the source and the receiver are placed at $(x_S, 0, z_S)$ and (x_R, y_R, z_R) respectively. The normalized admittances of the two vertical walls, ceiling and ground are β_{w1}, β_{w2}, β_c and β_f respectively.

All the image sources are presented as $(x_m, 0, z_n)$, where *m* is the location parameter of the image source along *x*-axis direction and *n* is the location parameter of the image source along *z*-axis direction respectively. Thus the ranges of m and n are $m \in (-\infty, +\infty)$ and $n \in (-\infty, +\infty)$. Given the values of m and n, the relation between the coordinates of certain image source $(x_m, 0, z_n)$ and m and n is determined as:

$$x_m = \begin{cases} (m+1)W - x_S & \text{for } m \text{ odd.} \\ mW + x_S & \text{for } m \text{ even.} \end{cases}, \quad z_n = \begin{cases} (n+1)H - z_S & \text{for } n \text{ odd.} \\ nH + z_S & \text{for } n \text{ even.} \end{cases} \tag{1}$$

When $m = 0$ and $n = 0$, $(x_m, 0, z_n)|_{m=0,n=0} = (x_S, 0, z_S)$. (2)

The space geometry relation between all sources (including image sources and actual sound sources) and the receiver is shown in Fig.2.

Given that $\Delta x = |x_m - x_R|, \Delta y = |y_R|, \Delta z = |z_n - z_R|$, the distance between the source and the receiver is $d_{mn} = \sqrt{\Delta x^2 + \Delta y^2 + \Delta z^2}$.

θ_1 is the incident angle of the sound ray (from the image source to the receiver) upon the plane parallel to the sidewalls. Similarly, θ_2 is the incident angle of the sound ray upon the plane parallel to the ceiling and ground. Thus θ_1 and θ_2 are presented as:

$$\theta_1 = \boldsymbol{arc}\cos\frac{\Delta \boldsymbol{x}}{\boldsymbol{d_{mn}}}, \theta_2 = \boldsymbol{arc}\cos\frac{\Delta \boldsymbol{z}}{\boldsymbol{d_{mn}}} \tag{3}$$

Given that β_{w1}, β_{w2}, β_c and β_f are the normalized admittances of the two parallel vertical walls, ceiling and ground, the plane wave reflection coefficients of the four planes can be obtained by [8-9]:

$$R_{w1} = \frac{\cos\theta_1 - \beta_{w1}}{\cos\theta_1 + \beta_{w1}} \ , \ R_{w2} = \frac{\cos\theta_1 - \beta_{w2}}{\cos\theta_1 + \beta_{w2}}$$
$$R_c = \frac{\cos\theta_2 - \beta_c}{\cos\theta_2 + \beta_c} \ , \ R_f = \frac{\cos\theta_2 - \beta_f}{\cos\theta_2 + \beta_f} \tag{4}$$

Then the loss factor of the four boundaries $F(w_{mnj})$ $(j = w1, w2, c, f)$ can be determined by [10-12]:

$$F(w_{mnj}) = 1 + i\sqrt{\pi} w_{mnj} e^{-w_{mnj}^2} \mathrm{erfc}(-i w_{mnj}) \tag{5}$$

with the parameter w_{mnj} defined by:

$$w_{mnj} = \sqrt{kd_{mn}/2}(1+i)(\cos\theta_1 + \beta_j) \quad (j = w1, w2) \tag{6}$$

$$w_{mnj} = \sqrt{kd_{mn}/2}(1+i)(\cos\theta_2 + \beta_j) \quad (j = c, f) \tag{7}$$

The combined complex wave reflection coefficient determined by d_{mn}, β_j and $F(w_{mnj})$ $(j = w1, w2, c, f)$ can be presented as [10-12]:

$$\begin{aligned} Q_1(m) \equiv Q(d_{mn}, \beta_j, \theta_1) &= R_j + (1-R_j)F(w_{mnj}) \quad \text{for } m \text{ odd}, \ j = w2. \\ &= R_j + (1-R_j)F(w_{mnj}) \quad \text{for } m \text{ even}, \ j = w1. \\ Q_2(n) \equiv Q(d_{mn}, \beta_j, \theta_2) &= R_j + (1-R_j)F(w_{mnj}) \quad \text{for } m \text{ odd}, \ j = c. \\ &= R_j + (1-R_j)F(w_{mnj}) \quad \text{for } m \text{ even}, \ j = f. \end{aligned} \tag{8}$$

Then the combined complex wave reflection coefficient is presented as:

$$Q_{s-mn} = \Pi Q_1(m) \Pi Q_2(n) \tag{9}$$

If location parameters $m > 0$ or $n > 0$, continued multiplication begins from the first order to the *m*th or *n*th order. If location parameters $m < 0$ or $n < 0$, continued multiplication begins from the zero order to the *m*th or *n*th order.

Then the sound field in a long enclosure can be computed by:

$$P = \frac{1}{4\pi} \sum_{m=-\infty}^{\infty} \sum_{n=-\infty}^{\infty} Q_{s-mn} \frac{e^{ikd_{mn}}}{d_{mn}} \tag{10}$$

With the introduction of the location parameters m and n, the spherical wave reflection coefficient of each order $Q_1(m)$ or $Q_2(n)$ can be accurately computed with the coherent model. Therefore, even when a long enclosure has boundaries with different impedance, the coherent model can still be used to investigate the sound field in a long enclosure with different impedance boundaries.

3.Numerical simulation and experiments

In this section, the theoretical results previously obtained are used for numerical simulation and experimental research on specific long enclosures. Although the coherent model can deal with the complex situation of four walls with different impedance in a long enclosure, here the sound field of a long enclosure with only one impedance boundary is studied. In presentation of the results of numerical simulation, the excess attenuation *EA* is used, which is defined as the logarithm of the ratio of the total sound field at various receivers P to the sound pressure at the source P_s.

$$EA = 20\log(P / P_s) \tag{11}$$

3.1 Experimental conditions

The long enclosure used in this experiment is made of density boards. With a sound absorption coefficient lower than 0.05 within the frequency range of 500~4000Hz adopted in this experiment, these density boards can be used to simulate rigid boundaries. The inner dimensions of the long enclosure are 9.8m long, 0.5m wide and 0.7m high. In the experiment, to reduce sound reflections, both ends of the long enclosure were attached with 20cm thick sound-absorbing wool with the absorption coefficient over 0.9 within the measurement frequency range of 500~4000Hz. One of the sidewalls of the long enclosure was attached with 5cm thick sound-absorbing wool to simulate the conditions of an impedance boundary with very high sound absorption performance. Therefore, the practicable dimensions of the long enclosure used in this experiment are 9.4m long, 0.45m wide and 0.7m high. Fig. 3 shows the schematic diagram of the long enclosure.

The microphone used in this experiment was fixed at different locations on a movable metal rack with nylon lines. As shown in fig. 4, the two test locations are both 0.35m high and 0.1m and 0.35m from the rigid boundary respectively.

3.2 Measurement of acoustic features of impedance material

When a boundary of the long enclosure is made of density boards, the normalized admittance of this boundary can be assumed to be $\beta = 0$. On the other hand, when a boundary of the long enclosure is an impedance boundary simulated with the sound-absorbing wool, the normalized admittance of this boundary should be measured in advance. In the experiment, B&K Pulse 3560D system was used to test the acoustic features of the sound-absorbing wool. As shown in fig. 5, the normal incidence sound absorption coefficient of the sound-absorbing wool shows that the sound-absorbing wool used in the experiment has higher sound absorption performance. The normalized admittances of the sound-absorbing wool used in both the experiment and numerical simulation at one-twelfth octave bands for frequencies from 500 Hz to 4000 Hz are listed in Table 1.

3.3 Discussion on ODEON prediction, numerical prediction and experimental results

When the source is located at (0.2, 0, 0.35), fix the microphone on the movable metal rack along the line of x = 0.35, z = 0.35. Fig. 6 shows the ODEON prediction, coherent model prediction, and experimental results of sound propagation along the line of x = 0.35, z = 0.35 at frequencies of 500Hz, 1000Hz, 2000Hz and 4000Hz.

When the source is located at (0.2, 0, 0.35), fix the microphone on the movable metal rack along the line of x = 0.1, z = 0.35. Fig. 7 shows the ODEON prediction, coherent model prediction, and experimental results of sound attenuation along the line of x = 0.1, z = 0.35 at frequencies of 500Hz, 1000Hz, 2000Hz and 4000Hz.

As shown in the figures, the coherent model developed in this paper can better simulate the trend of sound propagation in the long enclosure. On the other hand, the curve of the ODEON predictions is almost flat, indicating the ODEON predictions cannot reflect the trend of sound attenuation in the long enclosure at different frequencies. Particularly, when at 500Hz, the results of the ODEON predictions are far away from those of both the coherent

model predictions and actual measurements. This is because the ODEON predictions are based on the sound ray theory, of which the results have a rather large deviation from those of actual measurements at low frequencies. Like many other ray tracing-based methods used in the past, the ODEON, from the statistical viewpoints, predicts the propagation model of the evenly distributed sound in the long enclosure at various frequencies, overlooking the effect of the fluctuation of sound waves at particular frequencies. On the basis of the wave theory-based image source model, the coherent model developed in the paper introduces the spherical wave reflection into the complex image source method, taking into consideration of the coherence of the sound waves. Thus the results of the coherent model prediction are better in line with those of the actual measurements.

However, there are still discrepancies between the coherent model predictions and the actual measurements. First, the combined complex wave reflection coefficient of the coherent model is based on the first order expansion, allowing the appearance of an extreme value point in the coherent model predictions. While in the coherent model, the predictions are only for a single frequency, there exist ambient noises at various frequencies in reality. The existence of these noises makes it impossible for the appearance of a peak value in theoretical predictions. Additionally, given the fact that, theoretically, the peak prediction distance is 10cm which is shorter than the actually measured interval distance, it is impossible to accurately obtain a peak value. Besides, judging from the experimental conditions, both ends of the long enclosure adopted in the experiment were attached with 20cm thick sound-absorbing wool to simulate full absorption, which is different from the assumption of full absorption in numerical simulation and is likely to have certain effect on the results.

4.Conclusions

Based on the research of [7], this paper has actualized a coherent model of the long enclosure and studied the sound attenuation along the long axis direction of a long enclosure with different impedance boundaries through computing the spherical wave reflection coefficient of each order in turn. Judging from the results of the ray-based ODEON prediction, coherent model prediction, and the measurement of experimental sound attenuation, the coherent model of the long enclosure developed in this paper predicts the trend of sound attenuation in long enclosure better than the traditional ODEON does.

References

[1] Kang J. The unsuitability of the classic acoustical theory in long enclosures. *Architect. Sci. Rev.*, 1996; **39**, 89-94
[2] Yamamoto T. On the distribution of sound in a corridor. *J. Acoust. Soc. Jpn.*, 1961; **17**, 286–292 (in Japanese)
[3] Redmore T. L. A theoretical analysis and experimental study of the behavior of sound in corridors. *Appl. Acoust.*, 1982; **15**, 161-170
[4] Sergeev M. V. Scattered sound and reverberation on city streets and in tunnels. *Sov. Phys. Acoust.*, 1979; **25**, 248–252
[5] Imaizumi H., Kunimatsu S., and Isei T. Sound propagation and speech transmission in a branching underground tunnel. *J. Acoust. Soc. Am.*, 2000; **108**(2), 632-642
[6] Lemire G. and Nicolas J. Aerial propagation of spherical sound waves in bounded spaces. *J. Acoust. Soc. Am.*, 1989; **86**, 1845-1853
[7] Li K. M. and Iu K. K. Propagation of sound in long enclosures. *J. Acoust. Soc. Am.*, 2004; **116**(5), 2759-2770
[8] Morse P.M. and Ingard K.U. Theoretical Acoustics, McGraw-Hill Book Company, New York. Morse, 1968
[9] Gensane M. Validité de la méthode des images en acoustique des salles. thesis, Faculté des sciences d'Aix-Marseille, France, 1978
[10] Kuttruff H. Room Acoustics, Applied Science Publishers Limited, London, 2nd edn., 1979
[11] Briquet M. and Filippi P. Diffraction of a spherical wave by an absorbing plane. *J. Acoust. Soc. Am.*, 1977; **61**, 640-646
[12] Embleton T. F. W. Tutorial on sound propagation outdoors. *J. Acoust. Soc. Am.*, 1996; **100**, 31-48

Figures

Figure 1：Reflection model of image sources in a rectangular long enclosure with different impedance boundaries

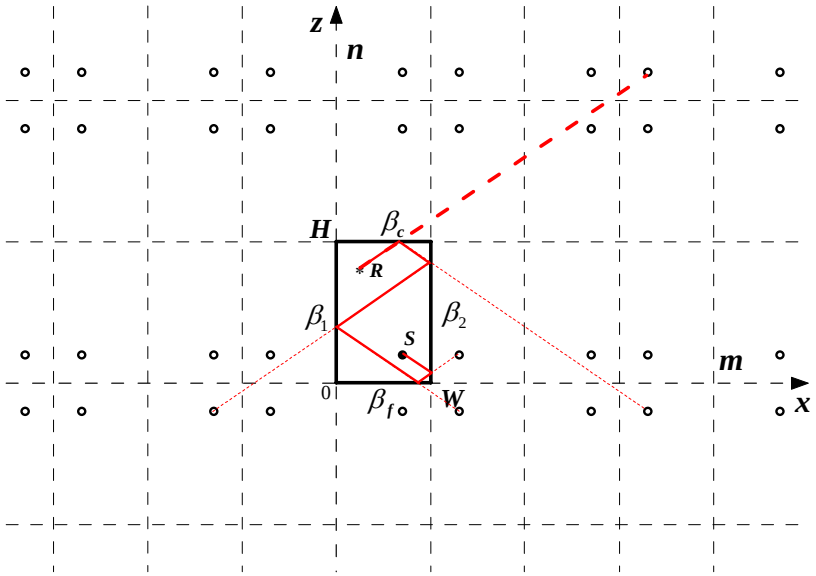

Figure 2：The space geometry relation between all sources and the receiver

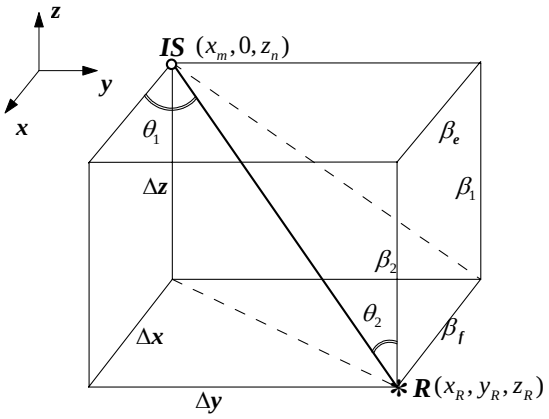

Figure 3：Schematic diagram of the long enclosure

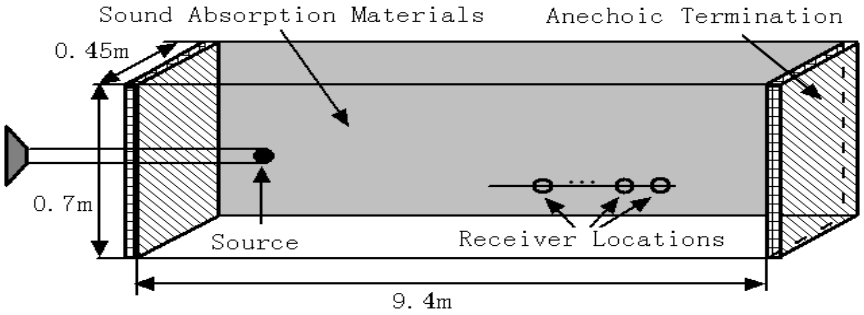

Figure 4：Two test locations on the movable metal rack

Figure 5：Sound absorption coefficient of the sound-absorbing wool

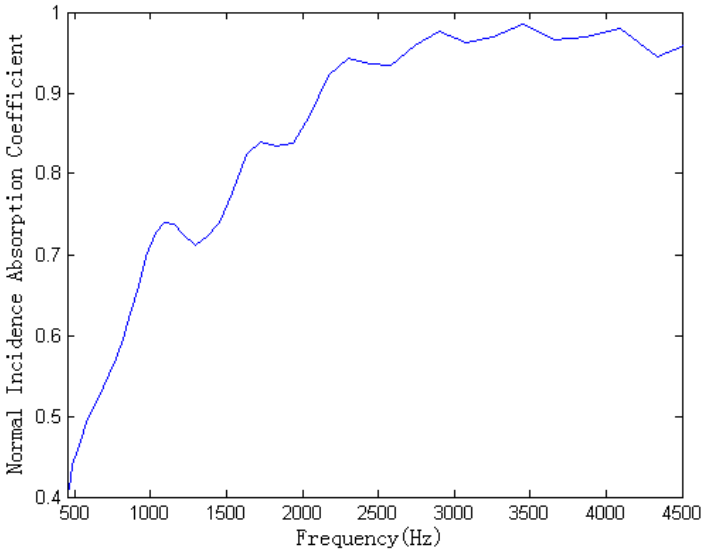

Figure 6：Comparison of ODEON prediction, theoretical prediction, and measurement results – source located at (0.2, 0, 0.35) ; receiver located along the line of x = 0.35, z = 0.35; frequencies at 500Hz, 1000Hz, 2000Hz and 4000Hz

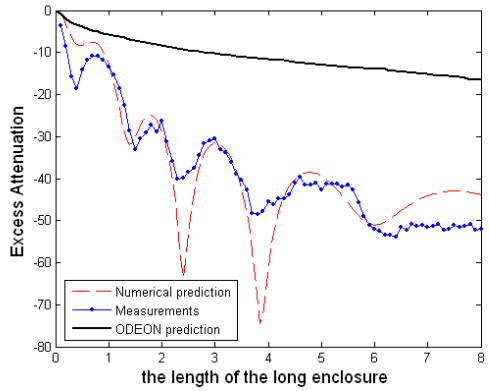

a) *f*=500Hz

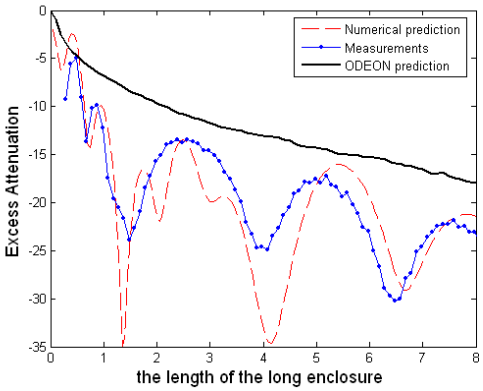

b) *f*=1000Hz

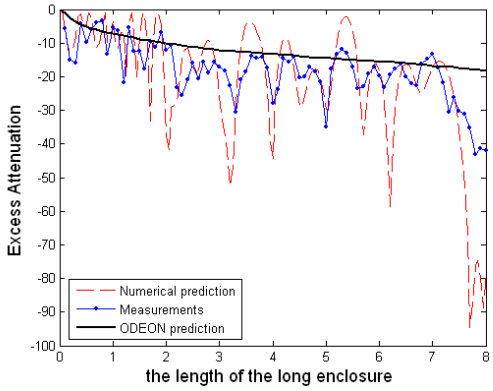

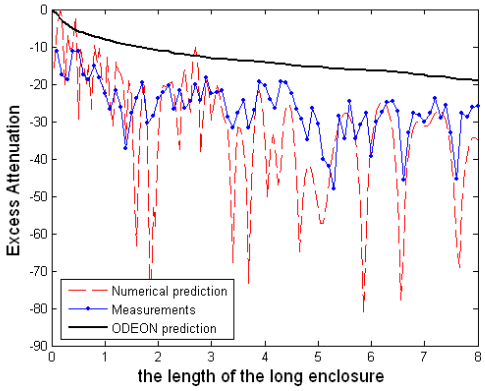

Figure 7：Comparison of ODEON prediction, theoretical prediction, and measurement results – source located at (0.2, 0, 0.35) ; receiver located along the line of x = 0.1, z = 0.35; frequencies at 500Hz, 1000Hz, 2000Hz and 4000Hz

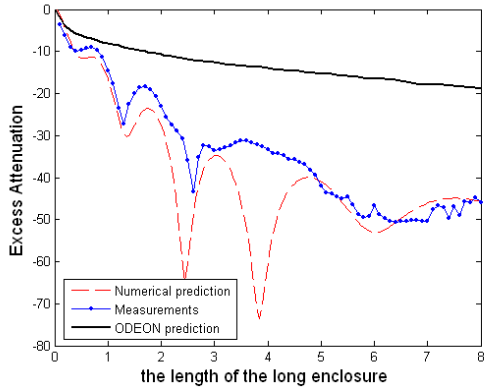

a) *f*=500Hz

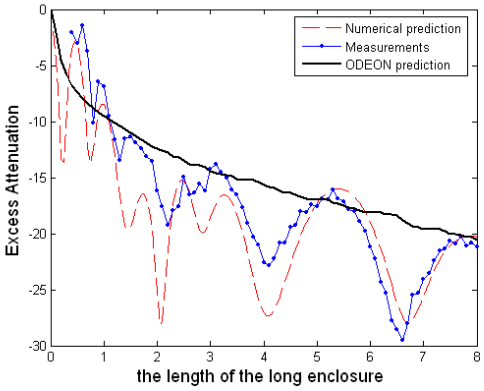

b) *f*=1000Hz

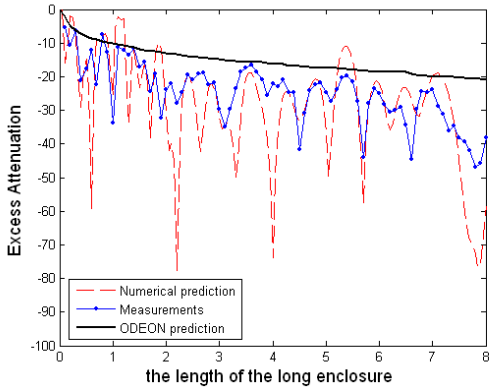

c) *f*=2000Hz

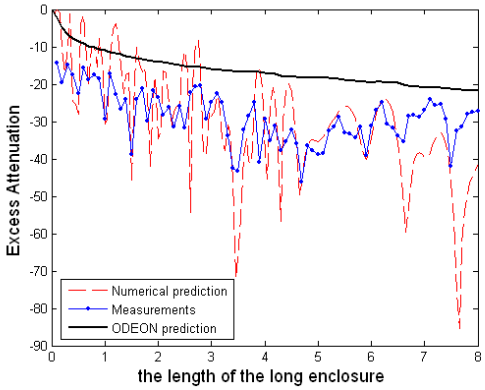

d) *f*=4000Hz

Tables

Table 1：Normalized admittances of the sound-absorbing material attached to the boundaries

Freq. (Hz)	Normalized admittances	Freq. (Hz)	Normalized admittances	Freq. (Hz)	Normalized admittances
459.73	7.5168 -	971.63	1.2068 -	2053.5	0.5062 +
486.97	5.4473 +	1029.2	2.9238 -	2175.2	0.5827 -
515.86	2.8702 +	1090.2	2.4221 +	2304.1	0.9561 -
546.39	1.5894 +	1154.8	0.7632 +	2440.6	1.6694 -
578.76	0.9646 +	1223.2	0.4588 +	2585.2	1.1813 +
613.06	0.6606 +	1295.7	0.3694 +	2738.4	0.7467 +
649.38	0.4885 +	1372.5	0.3145 +	2900.7	0.7916 -
687.86	0.3783 +	1453.8	0.3566 -	3072.6	1.3373 -
728.62	0.3020 +	1539.9	0.5052 -	3254.6	1.2199 +
771.79	0.2588 +	1631.2	1.0617 -	3447.5	0.7865 +
817.52	0.2432 +	1727.8	2.3045 -	3651.7	1.0297 -
865.96	0.2459 +	1830.2	1.3695 +	3868.1	1.3758 +
917.28	0.2846 -	1938.7	0.6740 +	4097.3	0.7579 +